

Landau level spectroscopy of Bi_2Te_3 I. Mohelský,^{1,2} A. Dubroka³, J. Wyzula², A. Slobodeniuk^{2,4}, G. Martinez,² Y. Krupko,^{2,5} B. A. Piot², O. Caha³, J. Humlíček,³ G. Bauer,⁶ G. Springholz,⁶ and M. Orlita^{2,4,*}¹*Institute of Physical Engineering, Brno University of Technology, Technická 2, 616 69, Brno, Czech Republic*²*Laboratoire National des Champs Magnétiques Intenses, CNRS-UGA-UPS-INSA-EMFL, 25 rue des Martyrs, 38042 Grenoble, France*³*Department of Condensed Matter Physics and Central European Institute of Technology, Masaryk University, Kotlářská 2, 611 37 Brno, Czech Republic*⁴*Charles University, Faculty of Mathematics and Physics, Ke Karlovu 5, 121 16 Prague 2, Czech Republic*⁵*Institut d'Electronique et des Systemes, UMR CNRS 5214, Université de Montpellier, 34000, Montpellier, France*⁶*Institut für Halbleiter- und Festkörperphysik, Johannes Kepler Universität, Altenbergerstrasse 69, 4040 Linz, Austria*

(Received 4 May 2020; accepted 21 July 2020; published 7 August 2020)

Here we report on Landau level spectroscopy in magnetic fields up to 34 T performed on a thin film of the topological insulator Bi_2Te_3 epitaxially grown on a BaF_2 substrate. The observed response is consistent with the picture of a direct-gap semiconductor in which charge carriers closely resemble massive Dirac particles. The fundamental band gap reaches $E_g = (175 \pm 5)$ meV at low temperatures and it is not located on the trigonal axis, thus displaying either sixfold or twelvefold valley degeneracy. Interestingly, our magneto-optical data do not indicate any band inversion at the direct gap. This suggests that the fundamental band gap is relatively distant from the Γ point where profound inversion exists and gives rise to the relativistic-like surface states of Bi_2Te_3 .

DOI: [10.1103/PhysRevB.102.085201](https://doi.org/10.1103/PhysRevB.102.085201)

I. INTRODUCTION

Bismuth telluride (Bi_2Te_3) is nowadays a widely explored material in the condensed-matter community. Intensive investigations of Bi_2Te_3 started more than 50 years ago and they were, to a great extent, driven by its remarkable thermoelectric properties [1–3]. More recently, Bi_2Te_3 appeared among the very first experimentally verified three-dimensional topological insulators which host a relativistic-type conical band on the surface [4–7]. Such surface states appear in Bi_2Te_3 due to band inversion at the center of the Brillouin zone where spin-orbit interaction reverses the order of p states as compared to isolated atoms of tellurium and bismuth [8].

Despite considerable experimental effort, the electronic band structure of Bi_2Te_3 is nowadays only partly understood. The current consensus implies that Bi_2Te_3 is a narrow-gap semiconductor. Nevertheless, the number and positions of extrema in the lowest-lying conduction and topmost valence bands, still remain under debate. Hence, it is still not clear whether the energy band gap is direct—with the extrema in the conduction and valence band aligned in the momentum space—or indirect.

From quantum oscillation experiments [9–15], it was concluded that six nonequivalent valleys exist both in the conduction as well as in the valence band, located pairwise in the mirror planes of Bi_2Te_3 (cf., Fig. 1). ARPES studies [5,16–19] also suggest multiple, likely sixfold [20], valley degeneracy in the valence band, but the minimum of the conduction band appears to be projected to the $\bar{\Gamma}$ point of the surface Brillouin zone. This implies either none or double valley degeneracy,

with the minimum at the Γ (Z) point or on the Γ - Z line, respectively. In optical experiments [21–28], both direct and indirect band gaps were reported with widths not exceeding 200 meV. Available theoretical studies provide us with diverse views on the electronic bands in Bi_2Te_3 [8,29–32]. Presumably more accurate *GW* calculations predict multiple extrema of the highest valence band and one or more valleys in the conduction band [33–37]. The calculated band gap thus can be both direct or indirect. Its magnitude depends on the used functional and falls into a relatively broad range of energies between 50 and 200 meV.

In this paper we study the bulk magneto-optical response of a thin layer of Bi_2Te_3 . We show that the relatively complex response, comprising a series of interband and intraband inter-Landau level (inter-LL) excitations, may be explained using a simple two-band model for a time-reversal-invariant direct-gap semiconductor. This implies that the charge carriers in Bi_2Te_3 behave, to a certain extent, as massive Dirac electrons. The selection rules for electric-dipole excitations observed experimentally allow us to deduce the symmetry of electronic bands around the fundamental band gap. In this way we conclude that the direct band gap is located away from the trigonal axis, and therefore, it displays a multiple degeneracy ($N = 6$ or 12).

II. SAMPLE PREPARATION AND EXPERIMENTAL DETAILS

The studied Bi_2Te_3 epilayer with a thickness of 300 nm was grown using molecular beam epitaxy on a 1-mm-thick (111)-oriented cleaved BaF_2 substrate [38,39]. The details about the growth technique and the sample characterization were presented previously [27]. The Hall measurements at

*milan.orldita@lncmi.cnrs.fr

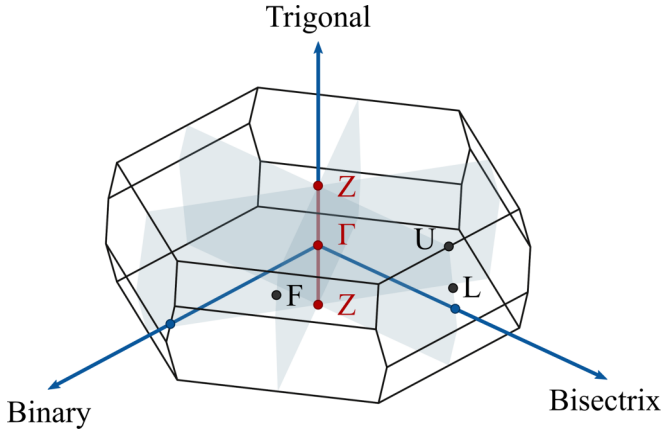


FIG. 1. Schematic view of the first Brillouin zone of Bi_2Te_3 with the mirror planes (gray planes) and trigonal, bisectrix as well as binary axes indicated.

liquid-helium temperature, performed on the same sample as all our optical and magneto-optical studies, indicate p -type conductivity and a moderate hole density of $p \sim 2 \times 10^{18} \text{ cm}^{-3}$.

To measure infrared magnetotransmission, nonpolarized radiation from a global or a mercury lamp was analyzed by a commercial Bruker Vertex 80v Fourier-transform spectrometer. The radiation was then delivered via light-pipe optics to the sample kept in the helium exchange gas at the temperature $T = 2 \text{ K}$ and placed in a superconducting solenoid or in the resistive high-field magnet (above 13 T, up to 34 T), both at the LNCMI in Grenoble. The light transmitted through the sample was detected by a composite bolometer, placed directly below the sample. The studied sample was probed in the Faraday configuration, with the magnetic field applied along the trigonal axis (rhombohedral or c axis) of Bi_2Te_3 . The measured transmission spectra T_B were normalized by the zero-field transmission T_0 , and plotted in the form of relative magnetotransmission T_B/T_0 or relative magnetoabsorbance $A_B = -\ln[T_B/T_0]$. The optical response at $B = 0$ was deduced from the ellipsometric measurements realized using a commercial Woollam IR-VASE ellipsometer coupled to a closed He-cycle cryostat, for details see Ref. [27].

III. TWO-BAND MODEL OF A DIRECT-GAP SEMICONDUCTOR

To interpret our experimental data presented and discussed below, we adopt a simple two-band model for a time-reversal-invariant direct-gap semiconductor. The corresponding Hamiltonian may be derived, e.g., using the first-order $\mathbf{k} \cdot \mathbf{p}$ theory applied at a particular point \mathbf{k}_0 of the Brillouin zone:

$$h = \begin{bmatrix} \Delta & \hbar v_D(q_x + iq_y) \\ \hbar v_D(q_x - iq_y) & -\Delta \end{bmatrix}, \quad (1)$$

where $\mathbf{q} = \mathbf{k} - \mathbf{k}_0 = (q_x, q_y, 0)$. The Hamiltonian describing electrons and holes with an opposite spin projection in the doubly degenerate bands is obtained by the complex

conjugation of h (h^*). Notably, we consider only vanishing q_z momenta because the $q_z = 0$ states dominate the overall optical response when the magnetic field is applied along the z axis.

The above Hamiltonian gives rise to the conduction and valence bands with a characteristic relativistic-like hyperbolic profile: $E(k) = \pm \sqrt{\Delta^2 + \hbar^2 v_D^2 k^2}$. They are separated by the band gap of 2Δ and display the full particle-hole symmetry. Interestingly, there exists a nontrivial analogy between the proposed two-band model and truly relativistic systems of massive electrons described by the Dirac equation [40–44]. This analogy implies that the band-edge effective masses of electrons and holes are equal to the quantity referred to as the Dirac mass, $m_D = m_e = m_h = \Delta/v_D$. The effective (cyclotron) mass of charge carriers increases linearly with the energy distance ε from the band edge: $m_{e,h}(\varepsilon) = m_D(1 + \varepsilon/\Delta) = m_D|E|/\Delta$. The corresponding g factors are expressed as $g_e = g_h = 2m_0/m_D$, where m_0 stands for the bare electron mass. For large momenta, the dispersion of charge carriers approaches the ultrarelativistic limit $E(\mathbf{k}) \approx \pm \hbar v_D |\mathbf{k}|$. This allows us to treat the v_D parameter which describes the coupling between bands, as the effective velocity of light in the explored system.

When a magnetic field is applied, the electronic band structure transforms into Landau levels with the spectrum: $E_n = \pm \sqrt{v_D^2 2e\hbar B n + \Delta^2}$, where $n > 0$. In addition, there exists a pair of spin-polarized zero-mode LLs ($n = 0$) with the energies $E_0 = \Delta$ and $E_0 = -\Delta$, which correspond to the h and h^* Hamiltonians, respectively. Our model, characterized by the full rotational symmetry around the z axis, implies the standard selection rules $n \rightarrow n \pm 1$ for electric-dipole excitations in the Faraday configuration (Fig. 2). A closer analysis [43,45] shows that the excitations within the LL spectra of the h and h^* Hamiltonians dominantly follow the selection rules $n \rightarrow n - 1$ and $n \rightarrow n + 1$ and they are active in σ^- and σ^+ polarized light, respectively. This remains valid until the energy of excitations exceeds, by an order of magnitude, the band gap of 2Δ .

Let us now reconcile the proposed toy model of massive Dirac electrons with the real band structure of Bi_2Te_3 . We align the z axis in the model with the trigonal axis of Bi_2Te_3 . The bands considered in the model are associated with the lowest lying conduction and the topmost valence bands which are primarily formed from p -like states of bismuth ($6p$) and tellurium ($5p$) [8,46]. The electronic bands at higher or lower energies are completely neglected. Even though we deal with a material proven to be a topological insulator [4–6], the band inversion, putting tellurium states above bismuth ones, does not have to be present around an arbitrarily chosen point \mathbf{k}_0 in the Brillouin zone, especially for the momenta far from the Γ point.

The position of the \mathbf{k}_0 point in the Brillouin zone (see Fig. 3) and the crystal symmetry imply the valley degeneracy N . When the possibility of an accidental degeneracy is neglected, the valley multiplicity reaches $N = 1$ when the \mathbf{k}_0 point coincides with the Γ or Z points (a half of the valley at both zone-boundary Z points), $N = 2$ for \mathbf{k}_0 located on the trigonal axis (between Z and Γ points), $N = 6$ for the

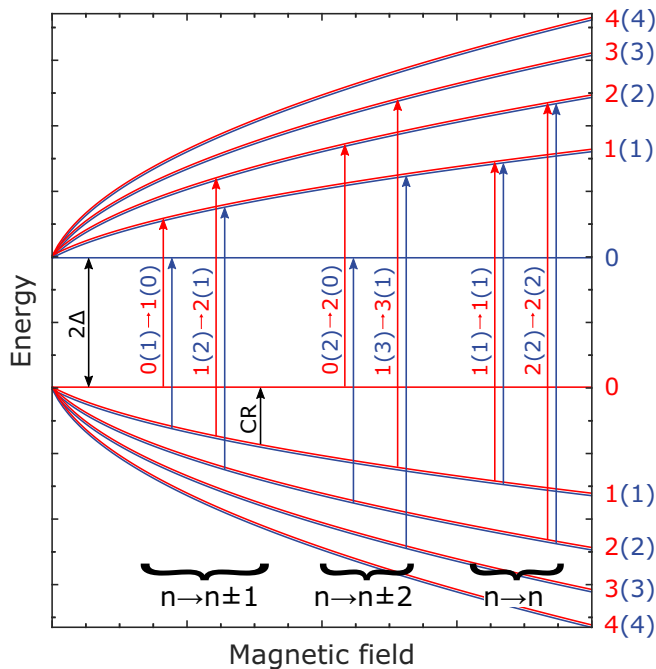


FIG. 2. Schematic view of the LL spectrum corresponding to the h and h^* Hamiltonians (blue and red, respectively). In the two-band model, the zero-mode ($n = 0$) LLs remain independent of B unless the Hamiltonians are expanded to include band inversion or the impact of higher/lower lying bands. The vertical arrows correspond to electric-dipole active transitions from three distinct sets. In the system with a full rotational symmetry around the c axis, only transitions $n \rightarrow n \pm 1$ may appear. CR denotes cyclotron resonance in the quantum limit of a p -type system. The $n \rightarrow n \pm 2$ excitations become active when the rotational symmetry is reduced to the trigonal one. When the symmetry is further reduced, transitions $n \rightarrow n$ may emerge.

valleys located in the mirror planes or on the binary axis (perpendicular to the trigonal axis), and $N = 12$ for a general position in the Brillouin zone [9].

Importantly, the symmetry of the crystal and the position of the \mathbf{k}_0 point in the Brillouin zone (see Fig. 1) may have a profound impact on the related magneto-optical response. The particular location of the \mathbf{k}_0 point in the Brillouin zone implies a specific form of high-order momentum terms that result from the $\mathbf{k} \cdot \mathbf{p}$ expansion. Often these terms do not impact the LL spectrum significantly and, therefore, they are not included in the Hamiltonian (1). Nevertheless, the lowered rotational symmetry gives rise, in principle, to additional sets of electric-dipole transitions.

For the point \mathbf{k}_0 located on the trigonal axis, the angular momentum of an absorbed photon is conserved only modulo 3 [45]. Therefore, additional sets of electric-dipole transitions may emerge in the excitations spectrum: $n \rightarrow n \pm 2, 5, 7, \dots$. The situation is similar to K point electrons in bulk graphite [47] for which the pronounced trigonal warping does not alter significantly the LL spectrum, but it gives rise to a series of cyclotron resonance (CR) harmonics that would be strictly forbidden in the electric-dipole approximation in a system with full rotational symmetry. Further sets of inter-LL excitations may appear for the \mathbf{k}_0 point located away from

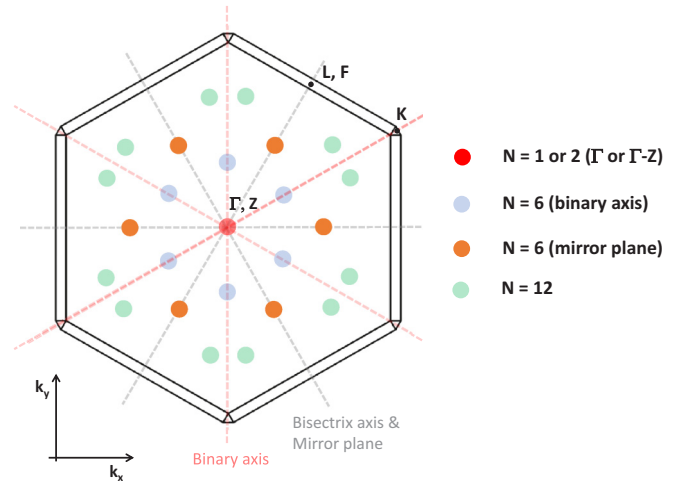


FIG. 3. The Brillouin zone of Bi_2Te_3 projected to the plane perpendicular to the trigonal axis. The full circles show possible positions of the band extrema, and their corresponding degeneracy, given by the crystal symmetry: at the Γ point or on the Γ - Z line ($N = 1$ or 2), in the mirror planes ($N = 6$), on the binary axes ($N = 6$) or in a general position ($N = 12$).

the trigonal axis of Bi_2Te_3 —for instance, interband transitions that conserve the LL index: $n \rightarrow n$.

IV. EXPERIMENTAL DATA AND DISCUSSION

The magneto-optical data collected on the studied Bi_2Te_3 epilayer at $T = 2$ K in the mid-infrared spectral range are presented in Figs. 4 and 5, as a stacked-plot and false-color plot of relative magnetoabsorbance spectra A_B , respectively. The data comprise a series of pronounced resonances that follow a sublinear in B dependence, and in the limit of the vanishing magnetic field, extrapolate to a finite (positive) energy. We interpret these resonances as inter-LL excitations that promote electrons across the band gap. The resonances have pronounced high-energy tails that are typical of interband inter-LL excitations in bulk systems.

A more detailed analysis shows the presence of additional transitions with a considerably weaker intensity. These latter transitions become clearly visible in the second derivative of the relative magnetoabsorbance, plotted as a false-color plot [Fig. 6(a)]. Since the observed resonances are relatively sharp, we associate the minima in $d^2A_B/d\omega^2$ curves directly with the positions of excitations [Fig. 6(b)]. Using the method of the second derivative, we also reduce the impact of the normalization by relatively flat zero-field transmission T_0 on the deduced energies of excitations. No resonances attributable to surface states were identified, in contrast to preceding studies [48].

Let us now compare our experimental data with expectations based on the proposed two-band model. In the first step we assign the series of dominant transitions, which contains up to eight well-resolved lines, with the position of $n \rightarrow n \pm 1$ resonances expected in a system with the full rotational symmetry. Very good agreement is found for an energy band gap $E_g = 2\Delta = (175 \pm 5)$ meV and a velocity parameter $v_D = (4.7 \pm 0.1) \times 10^5$ m/s, as shown by solid

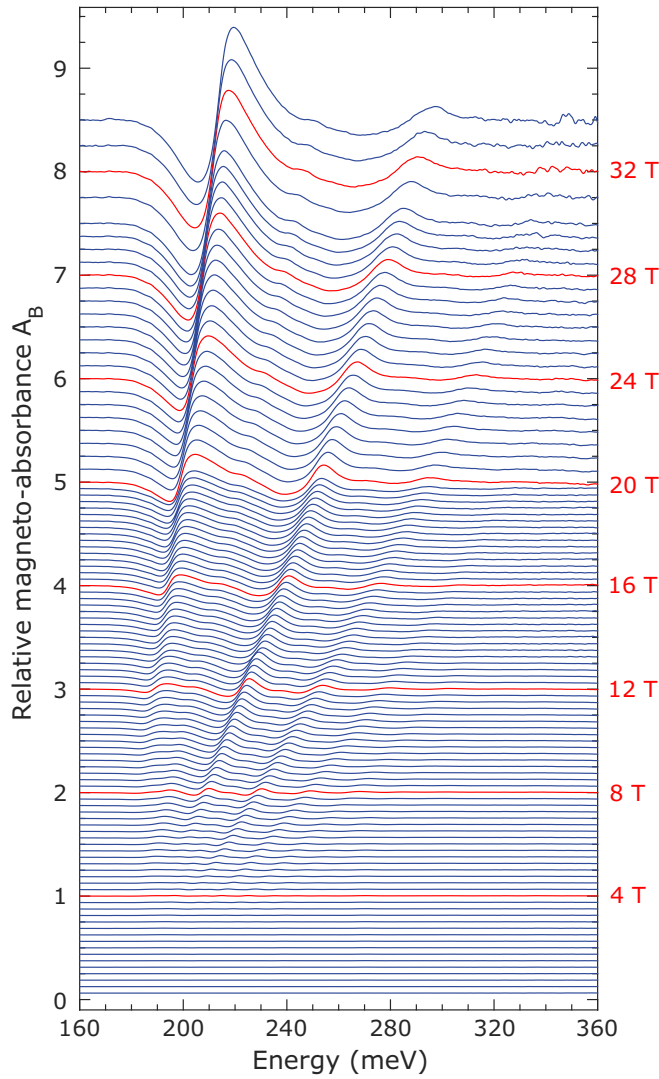


FIG. 4. Relative magnetoabsorbance spectra $A_B = -\ln[T_B/T_0]$ plotted for selected values of the applied magnetic field. The maxima correspond to individual inter-LL resonances. The minima (negative values of A_B) emerge due to suppression of zero-field absorption. A baseline-line correction has been performed (subtraction of a linear background) to ensure $T_B/T_0 \approx 1$ in the spectral range where no inter-LL excitations were observed (at high and low photon energies). Afterwards, the baseline of each spectrum has been shifted vertically by the offset of $0.25 \times B$ [T].

lines in Fig. 6(b). In this way, all dominant lines may be explained using only one widely tunable parameter v_D . This is because the band gap 2Δ falls into a fairly narrow interval given by the zero-field extrapolation of lines.

The parameters Δ and v_D deduced from the fit of dominant interband transitions allows us to predict the position and B dependence of the fundamental CR mode $1 \rightarrow 0$ in our p -type sample (cf., Fig. 2). This may be compared to the experimentally observed CR mode visible as a broad minimum in T_B/T_0 curves or the maximum in the false-color plot of relative magnetoabsorbance A_B [Figs. 7(a) and 7(b), respectively]. Moreover, the expected position [red solid line in Fig. 7(b)] matches very well the experimental data without

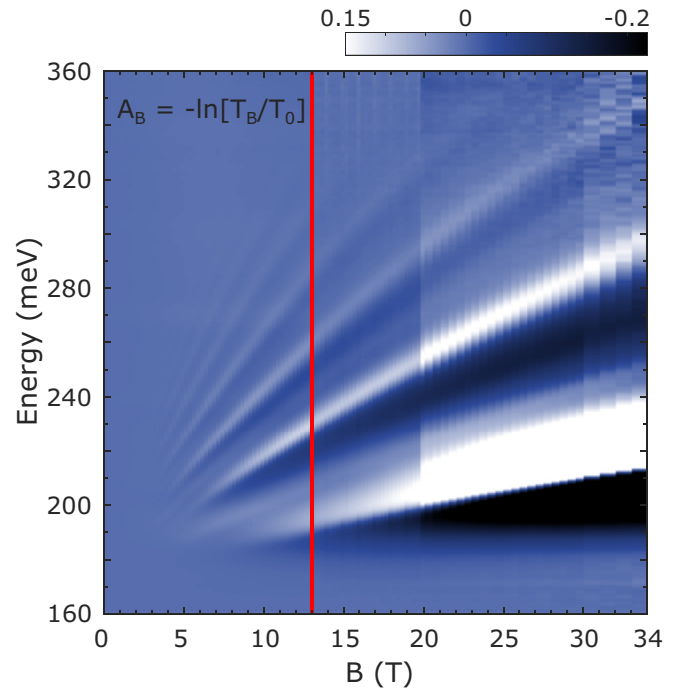


FIG. 5. Relative magnetoabsorbance A_B from Fig. 4, visualized as a false-color plot. The vertical red line separates the data collected using the superconducting and resistive coils, below and above 13 T, respectively.

any additional adjustment of v_D or Δ . The cyclotron energy deviates only weakly from a linear dependence in B . This allows us to describe it approximately by the formula for the cyclotron energy of a parabolically dispersing particle: $\hbar\omega_c = \hbar eB/m_D$ using the Dirac mass of $m_D = 0.07m_0$ [dashed gray line in Fig. 7(b)]. This value is in very good agreement with preceding studies which reported the band-edge mass of $0.08m_0$ [12,49]. Let us note that the observed CR mode indicates a coupling with optical phonons that may resemble the magnetopolaron effect [50,51]. Nevertheless, a relatively broad CR line, as compared to much sharper phonon resonances, does not allow us to analyze this effect in detail.

Importantly, our model does not include any electron-hole asymmetry. The experimentally deduced Dirac mass m_D thus represents a good estimate of the band-edge mass for both holes and electrons. Indeed, the extracted Dirac mass of $m_D = 0.07m_0$ is close to the electron band-edge mass of $0.06m_0$ deduced in quantum oscillation experiments in the past [11]. Importantly, this latter agreement indicates that the conduction-band minimum, hosting the final states of the observed interband inter-LL excitations, is not just a local extremum, but the global one. The parameter 2Δ thus corresponds to the fundamental band gap in Bi_2Te_3 . Hypothetically, one can imagine that there exist other extrema of the conduction and valence bands, which are characterized by the band-edge masses identical to the ones of valleys probed in our magneto-optical experiments. In such a case, the real energy band gap might still be smaller and indirect. However, we do not find such a coincidence probable.

The very good agreement between experimental data and our simple two-band model suggests that Bi_2Te_3 is a

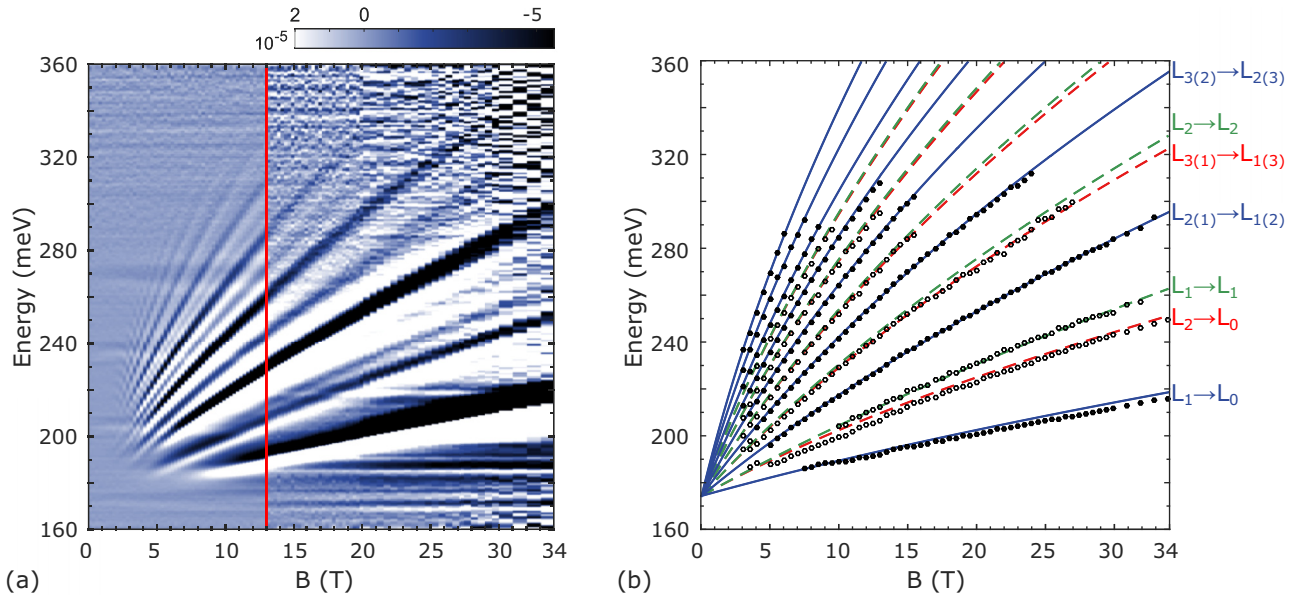


FIG. 6. (a) False-color plot of the second derivative of relative magnetoabsorbance in the middle infrared spectral range $d^2A_B/d\omega^2$. The vertical red line separates the data collected using the superconducting and resistive coils, below and above 13 T, respectively. (b) The deduced minima of $d^2A_B/d\omega^2$ associated with the positions of interband inter-LL excitations. The solid (open) circles correspond to positions of dominant (weak) lines in the spectra. The lines correspond to the theoretically expected positions of resonances that follow three different selection rules: $n \rightarrow n \pm 1$ (solid blue line), $n \rightarrow n \pm 0$ (dashed green line), and $n \rightarrow n \pm 2$ (dashed red line).

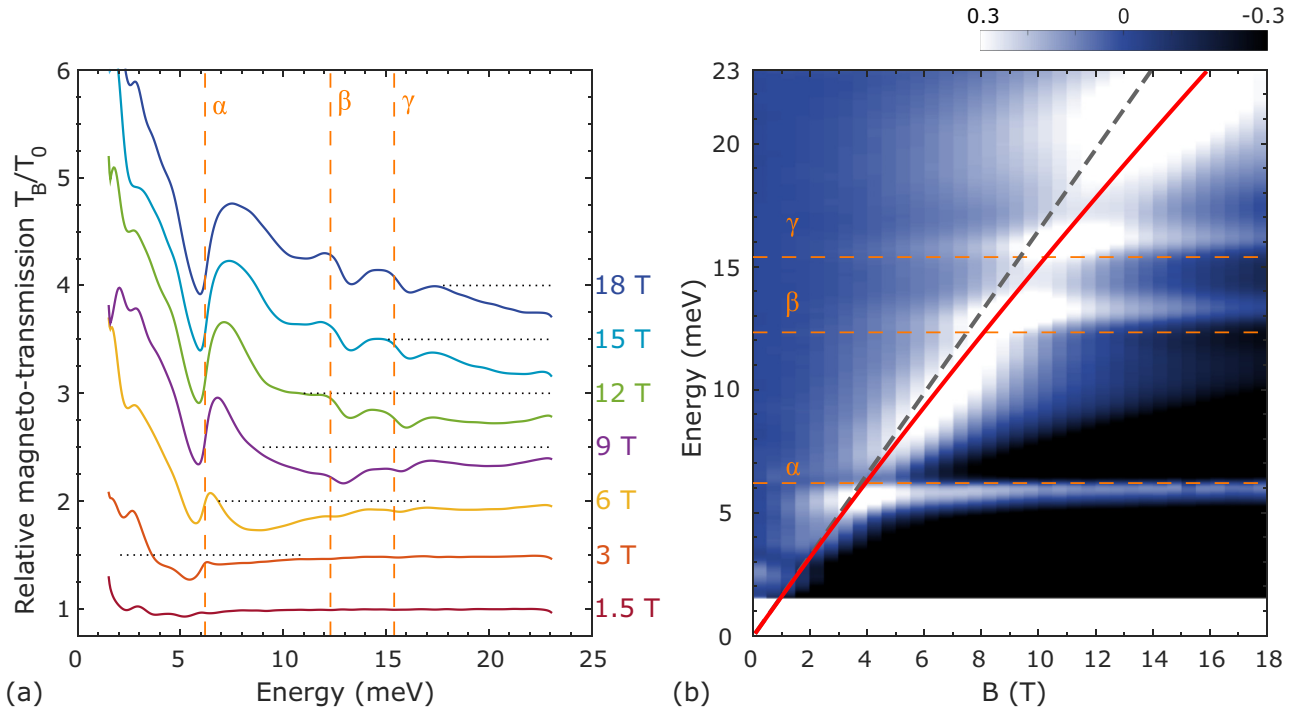


FIG. 7. (a) Relative magnetotransmission spectra T_B/T_0 plotted for selected values of B . The CR resonance absorption is manifested by a relatively broad minimum that shifts almost linearly with B towards higher energies. The pronounced B -induced transmission at low photon energies ($T_B/T_0 > 1$) is typical of the CR response in the quasiclassical regime (see, e.g., [52]). This is due to Drude-type absorption which dominates the response at $B = 0$ and which is suppressed by the applied magnetic field. The horizontal dotted lines show $T_B/T_0 = 1$ level for each stacked spectrum. (b) False-color plot of relative magnetoabsorbance A_B in the far infrared range. The solid red line corresponds to the energy of the fundamental CR mode $1 \rightarrow 0$ calculated within the two-band model (cf., Fig. 2). The dashed gray line shows the cyclotron energy $\hbar\omega_c = \hbar eB/m_D$ for the band-edge (Dirac) mass $m = \Delta/v_D^2 = 0.07m_0$. The vertical and horizontal dashed lines in (a) and (b), respectively, show positions of three phonon modes (α , β , and γ) observed in zero-field transmission spectrum. One may associate them with E_u^1 , E_u^2 , and A_{1u} infrared-active phonons [53]. The possible coupling between these phonons and CR mode is discussed in the main text. The last mode is supposed to be active for the electric-field component along the c axis, and it appears since the radiation is focused on the sample using a cone.

direct-gap semiconductor. However, one can never exclude a small displacement δk_{c-v} between the extrema of the conduction and valence bands. Thanks to our low-field magneto-optical data, we may find the upper limit of such a displacement. It is approximately given by the reciprocal value of the magnetic length $\delta k_{c-v} \sim 1/l_B = \sqrt{eB/\hbar} \approx 0.07 \text{ nm}^{-1}$, taken at the onset of LL quantization in our sample ($B \approx 3 \text{ T}$). Such a distance represents only a small fraction of the whole Brillouin zone size. This allows us to speak about the direct character of the band gap in Bi_2Te_3 with reasonable justification.

The validity of the proposed model also implies that the Zeeman splitting in Bi_2Te_3 should be equal to cyclotron energy $E_Z = E_C$ that is typical of massive Dirac electrons [54,55] and the g factors of electrons and holes should reach $g_e = g_h = 2m_0/m_D \approx 30$. In fact, large values of g factors are expected in systems composed of heavy elements with strong spin-orbit coupling [56,57]. To the best of our knowledge, no results from spin-resonance experiments on Bi_2Te_3 have been reported so far. Relatively large values for g factors were estimated from quantum oscillation experiments [11,13,15,58], but the concluded ratio was somewhat lower than unity: $E_Z/E_C \approx 0.5\text{--}0.7$. The difference may be attributed to the influence of more distant bands [59].

In a second step, we compare the positions of additional lines—with weaker integral intensities but still clearly manifested in the spectra—with the energies of other possibly existing inter-LL excitations. As a matter of fact, all additionally observed lines fit very well to two series: $n \rightarrow n \pm 2$ and $n \rightarrow n$ marked by dashed lines in Fig. 6(b). These two series nearly overlap for higher indices n , nevertheless, at low photon energies, one may clearly distinguish two separate $2 \rightarrow 0$ and $1 \rightarrow 1$ lines. Let us notice that the $0 \rightarrow 2$ transition should not appear due to the occupation effect in our p -type sample. The proposed two-band model, implying not more than two tunable parameters, is thus capable of explaining all intraband and interband inter-LL excitations resolved in our magneto-optical data (more than 10 lines). This strongly corroborates our interpretation.

The additionally appearing inter-LL excitations reflect the symmetry of electronic bands at the fundamental band gap. The presence of the $n \rightarrow n$ series indicates that the symmetry is definitely lower than the trigonal one. The direct fundamental gap, evidenced in our magneto-optical experiment, thus cannot be located on the trigonal axis of Bi_2Te_3 and the valley degeneracy must reach either $N = 6$ or $N = 12$, unless some accidental degeneracy occurs. Both possibilities have been discussed in the literature. The former one, corresponding to the energy gap within the mirror planes of Bi_2Te_3 (see Fig. 1), has been concluded as more probable based on quantum oscillations experiments [10–13,60], which followed the response for various orientations of the applied magnetic field with respect to crystallographic axes.

Let us confront our conclusions—about the size, nature, and multiplicity of the fundamental band gap in Bi_2Te_3 —with the zero-field optical response obtained using ellipsometry. In line with expectations, the deduced optical conductivity (Fig. 8) shows a rather steep increase at photon energies slightly above the band gap $E_g = 175 \text{ meV}$ estimated from our magneto-optical experiments. The optical response indicated

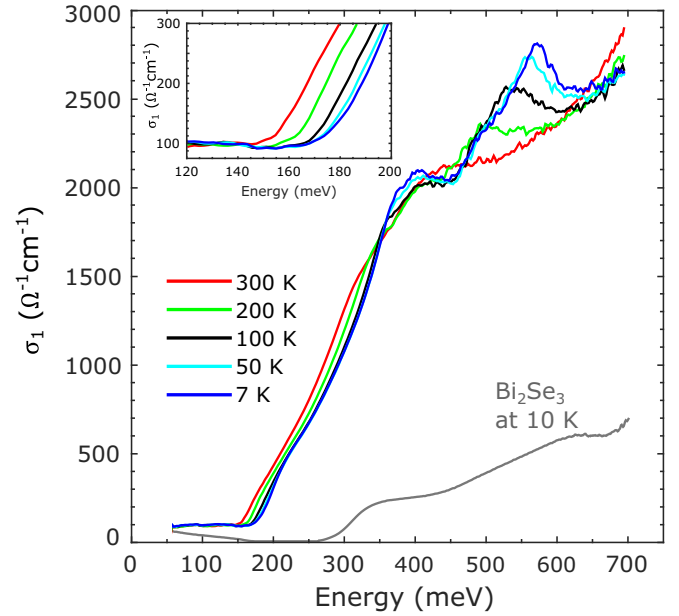


FIG. 8. The real part of optical conductivity $\sigma_1(\omega)$ of the studied Bi_2Te_3 sample at the selected temperatures measured using the ellipsometry technique. The inset shows in detail the sharp increase of $\sigma_1(\omega)$ due to the onset of interband excitations in Bi_2Te_3 at selected temperatures. For comparison, the optical conductivity spectrum of Bi_2Se_3 has been reprinted from [27], see the main text. Due to the Moss-Burstein effect [61,62], the onset of interband absorption is around 300 meV in this particular Bi_2Se_3 sample, which is well above the energy band gap of 220 meV [62].

the presence of several critical points in the explored part of the infrared spectral range, which are discussed in the Appendix. The lowest one, located around $E_g^* \sim 188 \text{ meV}$, corresponds to the onset of interband absorption, the so-called optical band gap. The difference $E_g^* - E_g$ is usually referred to as the Moss-Burstein (MB) shift [61], which is characteristic of all direct-gap degenerate semiconductors and which allows us to estimate the Fermi energy in our sample. Assuming the full particle-hole symmetry, we obtain E_F below 10 meV. This result is consistent with the Fermi energies found in quantum oscillations experiments performed on Bi_2Te_3 crystals with similar hole densities [12].

Similar to conventional semiconductors, the position of the absorption onset shifts to lower energies with increasing T (inset of Fig. 8). In this way we may estimate that, at higher temperatures, the energy band gap shrinks roughly linearly with T : $E_g \text{ (meV)} \approx 175 - 0.07 \times T \text{ [K]}$. Interestingly, the optical conductivity remains nonzero, nearly temperature independent, and flat at photon energies below E_g^* . This may be assigned to excitations from/to localized states in the band gap, but also, to the absorption tail of the (bulk) free holes whose scattering rate at these frequencies may be limited by disorder.

Above the optical band gap, $\sigma_1(\omega)$ in Bi_2Te_3 reaches significantly larger values as compared to the sister compound Bi_2Se_3 (see Fig. 8 and Ref. [27]). The latter has an inverted direct band gap with only a slightly higher width, located at the Γ point ($N = 1$) [62], and the electronic bands are also fairly well described by the Dirac Hamiltonian for

massive electrons [43]. The difference in $\sigma_1(\omega)$ thus must lie in specific band structure parameters—the reduced mass $\mu = m_e m_h / (m_e + m_h)$ and/or the valley degeneracy N , in particular. Assuming strictly parabolic profiles of bands, the optical conductivity can be approximated using the textbook expression for a direct-gap semiconductor [63]:

$$\sigma_1(\omega) \propto N \mu^{3/2} \sqrt{\hbar\omega - E_g}. \quad (2)$$

Comparing the reduced masses only, $\mu_{\text{Bi}_2\text{Se}_3} = 0.08m_0$ and $\mu_{\text{Bi}_2\text{Te}_3} = 0.035m_0$, one expects greater σ_1 for Bi_2Se_3 , roughly by a factor of 3. In experimental data, however, an opposite behavior is observed (Fig. 8). Above the corresponding optical band gaps, $\sigma_1(\omega)$ for Bi_2Se_3 is roughly by a factor of 5 smaller as compared to Bi_2Te_3 .

This opposite trend, as compared to the one with effective masses, is to a big part due to the large degeneracy N , thus confirming the multivalley nature of the band gap concluded in magnetotransport studies [10–13]. A simple argumentation based on Eq. (2) and the overall observed absorption would favorize the degeneracy $N = 12$ over 6. However, we stay rather conservative about this conclusion due to several other possible factors influencing the magnitude of absorption.

First, the impact of the pronounced anisotropy along the c axis ($\mu^{3/2} \rightarrow \mu_{\parallel} \mu_c^{1/2}$) was completely neglected. The anisotropy in Bi_2Te_3 may considerably differ from that in Bi_2Se_3 and it cannot be deduced from the presented magneto-optical data, which provide us only with the in-plane (i.e., perpendicular to the trigonal axis) estimate of the velocity parameter/effective mass.

Second, and likely more importantly, the absorption can be influenced by a nonparabolicity of the bands. Particularly in Bi_2Te_3 , a large nonparabolicity of the conduction band (flattening) was observed 20–30 meV above the band edge [11–13]. This large flattening, and the corresponding increase of the joint density of states, may enhance the absorption considerably. This could make the optical data compatible with the $N = 6$ valley degeneracy that was concluded, for both the conduction and valence bands, in de Haas–van Alphen and Shubnikov–de Haas studies [10–13].

Combining this sixfold-degeneracy deduced from quantum oscillations with the direct band gap deduced from magneto-optics, we may schematically sketch the profile of the conduction and valence bands as a function of the momentum along a line belonging to a mirror plane, but different from the trigonal axis (Fig. 9). This drawing respects the possible presence of a local minimum of the bulk conduction band at the Γ point indicated by some ARPES studies.

The applicability of the simple massive Dirac model to the magneto-optical response of Bi_2Te_3 may be somewhat surprising. In fact, the generic two-band models for 2D or 3D topological insulators [8,46,64,65] always comprise quadratic dispersive diagonal elements $\Delta \rightarrow \Delta + Mk^2$ which account for the band inversion ($\Delta \cdot M < 0$). Such dispersive diagonal elements are responsible for the appearance of the surface states, but they also profoundly impact bulk properties. For instance, when the magnetic field is applied, they lead to characteristic (anti)crossing of zero-mode ($n = 0$) LLs in all inverted systems [43,65–68].

Even though Bi_2Te_3 is a topological insulator—with experimentally confirmed surface states [4–6]—such diagonal

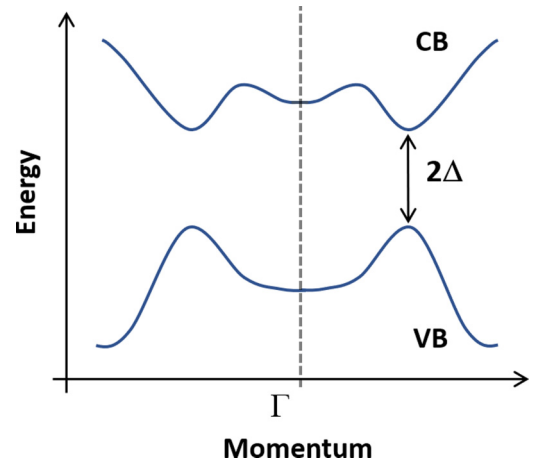


FIG. 9. Schematic drawing of a profile of the lowest conduction and topmost valence band (CB and VB) with a direct band gap and global extrema located away from Γ point that is consistent with our findings, but also with conclusions of magnetotransport experiments and ARPES data. The momentum is measured along the line within the mirror planes of Bi_2Te_3 different from the c axis.

dispersive terms are not included in our model, which thus keeps the simplest possible massive-Dirac form. This is, for instance, seen from the deduced electron and hole masses that approach very well the Dirac mass m_D . This contrasts with Bi_2Se_3 , where the massive Dirac picture is also valid [43], nevertheless, the presence of the dispersive diagonal elements in the Hamiltonian enhances the mass of electrons and holes by a factor of 2 as compared to the Dirac mass.

Let us emphasize that the absence of the dispersive terms on the diagonal of the Hamiltonian (1) is in line with findings of theoretical studies (see, e.g., [34,37]). These indicate that the band inversion is present only in a relatively narrow momentum range around the center of the Brillouin zone. The locations of the fundamental band gap thus does not have to coincide with the region of the band inversion, which is located at Γ point and which gives rise to the conical band on the surface (consequently centered at the $\bar{\Gamma}$ point of the surface Brillouin zone).

Another implication of the noninverted direct band gap in Bi_2Te_3 is that the velocity parameter v_D deduced from our experiments is not the one which determines the slope of the Dirac cones on the surface. Again, this is in contrast to other topological insulators such as Bi_2Se_3 or $\text{Bi}_{1-x}\text{Sb}_x$ where the regions of the fundamental band gap and of the band inversion overlap, and where the slope of the surface conical band provides us with a good estimate for the velocity parameter in the Hamiltonian describing bulk states.

V. CONCLUSIONS

We conclude that bismuth telluride is a direct-gap semiconductor with the band gap of $E_g = (175 \pm 5)$ meV at low temperatures. The performed analysis of the magneto-optical response implies that the fundamental band gap is not located on the trigonal axis, which implies its multiple degeneracy ($N = 6$ or 12). This conclusion corresponds well with findings of quantum oscillations experiments which indicate the valley

degeneracy $N = 6$ for both electrons and holes, located in the mirror planes [10–13]. We also conclude that the low-energy electronic excitations in Bi_2Te_3 are fairly well described within the model of massive Dirac electrons, which comprises only two material parameters.

ACKNOWLEDGMENTS

The authors acknowledge helpful discussions with I. Aguilera, D. M. Basko, M. Potemski, and J. Sanchez-Barriga. This work was financially supported by the European Regional Development Fund Project CEITEC Nano+ (No. CZ.021.01/0.0/0.0/16_013/0001728). CzechNanoLab project LM2018110 funded by MEYS CR is also gratefully acknowledged for the financial support of the measurements at CEITEC Nano Research Infrastructure. This work was supported by the ANR DIRAC3D project (ANR-17-CE30-0023). A.D. acknowledges support by the Czech Science Foundation (GAČR) under Project No. GA20-10377S and G.S. by the Austrian Science Fund FWF (Project No. I 4493). The authors also acknowledge the support of LNCMI-CNRS, a member of the European Magnetic Field Laboratory (EMFL).

APPENDIX

To complement the magneto-optical experiments, we have also performed ellipsometric measurements in the infrared spectral range and analyzed the obtained data using the approach adopted in our preceding study [27]. The modeling of the optical response enabled us to determine the thickness of the film (300 nm) and the thickness of the surface roughness effective layer. As a second step, the point by point dielectric function was obtained. The deduced real and imaginary part of the dielectric function $\varepsilon = \varepsilon_1 + i\varepsilon_2$ is shown in Fig. 10(a). The related real part of the low-temperature optical conductivity $\sigma_1 = \varepsilon_0\omega\varepsilon_2$ is shown in Fig. 10(b).

We have analyzed the interband transitions using the critical point (CP) model [69–71] that is widely applied to the second (or third) derivative of the dielectric function in order to enhance the CPs with respect to the background. The contribution of a parabolic CP to the second derivative is modeled as

$$\frac{d^2\varepsilon}{dE^2} = Ae^{i\phi}(E - E_{\text{CP}} + i\zeta)^{n-2}, \quad (\text{A1})$$

where A is the amplitude, E_{CP} is the energy, ζ is the broadening, and ϕ is the phase factor. The exponent n has the values $1/2, 0, -1/2$ for three-, two- and one-dimensional CP, respectively. In the simplest case of uncorrelated one-electron bands, the phase ϕ takes values of the integer multiples of $\pi/2$. For $A > 0$ and 3D critical point ($n = 1/2$), the phases $\phi = 0, 90, 180,$ and 270 deg correspond to $M_1, M_2, M_3,$ and M_0 critical points, respectively. For $A > 0$ and a 2D critical point ($n = 0$), $\phi = 0, 90,$ and 180 deg correspond to a minimum (M_0), saddle point (M_1), and maximum (M_2), respectively [70]. However, note that the phase can depart from these integer values for various reasons, e.g., when excitonic effects take place [72].

The model spectrum fitted to the second derivative of the real and imaginary part of the dielectric function is displayed in Fig. 10(c) and the obtained values of parameters are shown

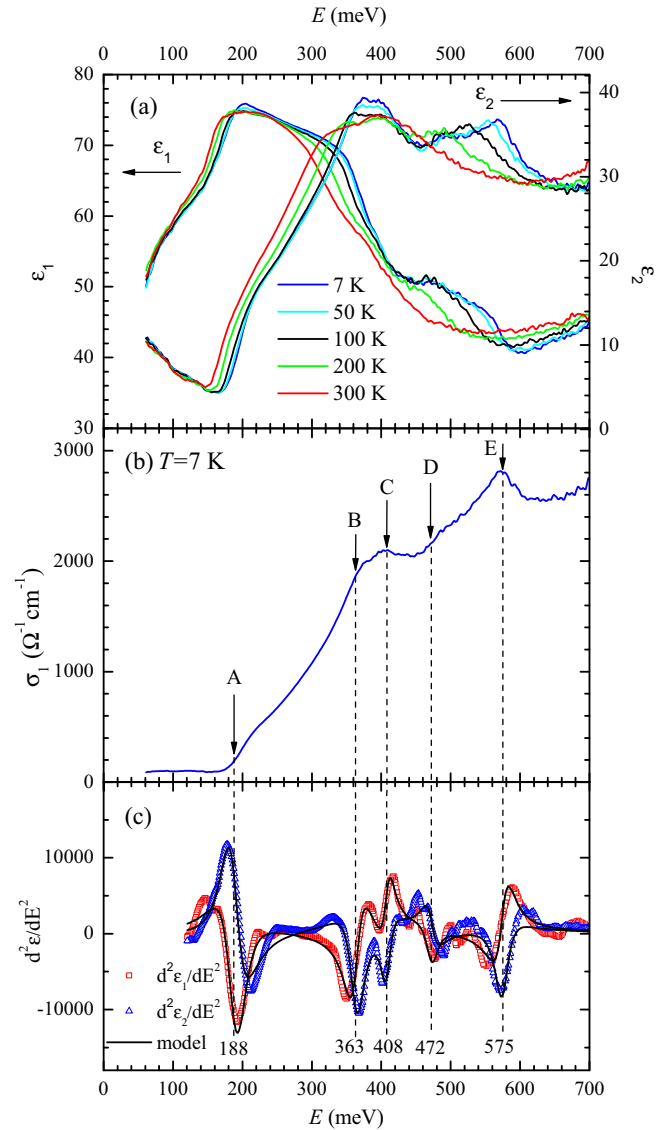


FIG. 10. Zero-field optical data obtained by ellipsometry. (a) The real and imaginary part of the dielectric function. (b) The real part of the optical conductivity at 7 K. The arrows denotes the critical points. (c) The second derivative of the real (red squares) and imaginary (blue triangles) part of the dielectric function and the model spectrum (black line). The numbers are the energies (in meV) of the related critical points.

in Table I. The main features of the second derivative are the same as the one reported in Ref. [27], however, here the higher quality of the sample, and consequently of the data, enabled us to resolve five critical points.

Concerning the critical point A at 188 meV, the best fit to the data was obtained using a 2D CP profile that is expected for the absorption edge influenced by the MB effect, see, e.g., the case of the Bi_2Se_3 thin film in Ref. [27]. Alternatively, this CP can be modeled with a 3D critical point (albeit with a minor increase in the mean square error) yielding $A = 30 \text{ eV}^{-1/2}$, $E_{\text{CP}} = 188 \text{ meV}$, $\zeta = 17 \text{ meV}$, and the phase $\phi = 285$ deg with a relatively minor departure from 270 deg of a simple M_0 CP. Obviously for a small MB shift in the

TABLE I. The values of the amplitude A , energy E_{CP} , broadening ζ , and phase ϕ obtained from the fit of the CP model to the data shown in Fig. 10(c).

Label	A	E_{CP} (meV)	ζ (meV)	ϕ (deg)	Line shape
A	7.8	188	24	-29	2D
B	$21 \text{ eV}^{-1/2}$	363	16	23	3D
C	$8 \text{ eV}^{-1/2}$	408	11	76	3D
D	$6 \text{ eV}^{-1/2}$	472	13	300	3D
E	$16 \text{ eV}^{-1/2}$	575	15	60	3D

same range as broadening ζ , a mixture of both types of critical points can be expected, which we believe is the case of the present data. Regardless of the dimensionality, the center energy of the lowest critical point is 188 meV, which is somewhat smaller than 202 meV reported on a similar sample in Ref. [27]. This is presumably caused by a lower doping and correspondingly smaller MB shift. Indeed, the square plasma frequency $4.4 \times 10^6 \text{ cm}^{-2}$ (as determined from the far-infrared reflectivity at 300 K, not shown) is smaller compared to the value of $5.4 \times 10^6 \text{ cm}^{-2}$ obtained on the sample studied in Ref. [27]. The values of ζ in the range of tens of meV are likely related to sample inhomogeneities, e.g., fluctuations of the local hole density and related fluctuations of the magnitude of the MB effect.

The CPs at higher energies were modeled with the 3D CP profiles. The phase values of CPs labeled as B and C (see Table I) suggest that they correspond to the M_1 and M_2 CPs, respectively, as expected following the M_0 CP. The phase of the critical point D is 300 deg, which is close to 270 deg and which suggests that it corresponds to M_0 CP. The phase of the critical point E is 60 deg, which is closest to the M_2 critical point. However, it is not excluded that the M_1 critical point is somewhat below this energy which effectively reduces the phase from 90 deg.

The presence of another CP is manifested in the magneto-optical data by appearance of a set of additional weak inter-LL transitions at higher energies (see Fig. 11). These correspond to excitations to/from a more distant band which is not included in the simplified model in the main text. The positions of these additional lines can be reproduced using an ad-hoc invoked massive Dirac Hamiltonian with the gap of 388 meV and the velocity parameter of $6 \times 10^5 \text{ m/s}$. This additional

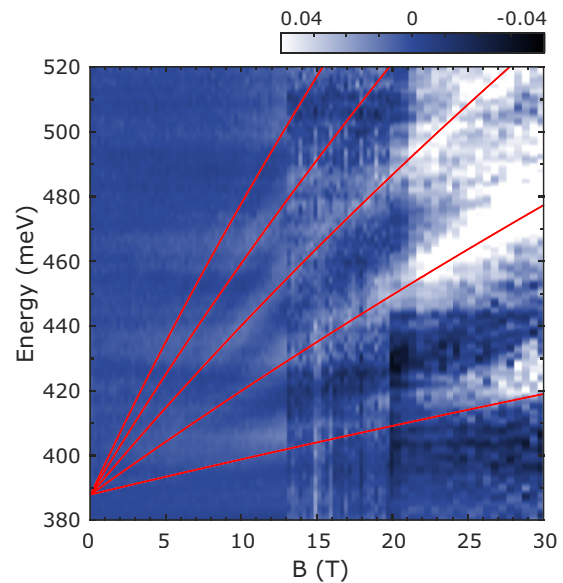


FIG. 11. False-color plot of relative magnetoabsorbance in the spectral interval well above the E_g . The observed series of inter-LL resonances promote electrons from/to a lower/higher lying band which is not included in the two-band model presented in the main text.

CP thus corresponds to another onset of interband excitations, and therefore, it should be of the 3D- M_0 type. Nevertheless, it is too weak to be identified directly in the zero-field optical response.

An intriguing question is whether one of experimentally identified CPs arises due to excitations at the Γ point. Inspecting the ARPES data [36], the onset of bulk interband transitions from the upward curved valence band to the conduction band is expected around the energy of 450 meV. Depending on the profile of the conduction and valence bands, the onset may give rise to a 3D critical point with a M_0 or M_3 character. In the given range of energies, we indeed find the critical point D which is of the M_0 type. Nevertheless, its assignment to the onset of interband excitations at the Γ point cannot be more than tentative at the moment. The ARPES data also suggest that there might be additional critical point(s) in the energy range of 300–400 meV, associated with transitions along the Z - Γ - Z axis, in line with our optical data.

[1] D. A. Wright, Thermoelectric properties of bismuth telluride and its alloys, *Nature (London)* **181**, 834 (1958).
 [2] H. J. Goldsmid, Bismuth telluride and its alloys as materials for thermoelectric generation, *Materials* **7**, 2577 (2014).
 [3] I. T. Witting, T. C. Chasapis, F. Ricci, M. Peters, N. A. Heinz, G. Hautier, and G. J. Snyder, The thermoelectric properties of bismuth telluride, *Adv. Electron. Mater.* **5**, 1800904 (2019).
 [4] D. Hsieh, Y. Xia, D. Qian, L. Wray, J. Dil, F. Meier, J. Osterwalder, L. Patthey, J. Checkelsky, N. P. Ong *et al.*, A tunable topological insulator in the spin helical Dirac transport regime, *Nature (London)* **460**, 1101 (2009).

[5] Y. L. Chen, J. G. Analytis, J.-H. Chu, Z. K. Liu, S.-K. Mo, X. L. Qi, H. J. Zhang, D. H. Lu, X. Dai, Z. Fang, S. C. Zhang, I. R. Fisher, Z. Hussain, and Z.-X. Shen, Experimental realization of a three-dimensional topological insulator, Bi_2Te_3 , *Science* **325**, 178 (2009).
 [6] D. Hsieh, Y. Xia, D. Qian, L. Wray, F. Meier, J. H. Dil, J. Osterwalder, L. Patthey, A. V. Fedorov, H. Lin, A. Bansil, D. Grauer, Y. S. Hor, R. J. Cava, and M. Z. Hasan, Observation of Time-Reversal-Protected Single-Dirac-Cone Topological-Insulator States in Bi_2Te_3 and Sb_2Te_3 , *Phys. Rev. Lett.* **103**, 146401 (2009).

- [7] M. Z. Hasan and C. L. Kane, Colloquium: Topological insulators, *Rev. Mod. Phys.* **82**, 3045 (2010).
- [8] H. Zhang, C.-X. Liu, X.-L. Qi, X. Dai, Z. Fang, and S.-C. Zhang, Topological insulators in Bi_2Se_3 , Bi_2Te_3 and Sb_2Te_3 with a single Dirac cone on the surface, *Nat. Phys.* **5**, 438 (2009).
- [9] J. R. Drabble and R. Wolfe, Anisotropic galvanomagnetic effects in semiconductors, *Proc. Phys. Soc. Sec. B* **69**, 1101 (1956).
- [10] R. B. Mallinson, J. A. Rayne, and R. W. Ure, de Haas-van Alphen effect in n -type Bi_2Te_3 , *Phys. Rev.* **175**, 1049 (1968).
- [11] H. Köhler, Non-parabolic $E(k)$ relation of the lowest conduction band in Bi_2Te_3 , *Phys. Status Solidi B* **73**, 95 (1976).
- [12] H. Köhler, Non-parabolicity of the highest valence band of Bi_2Te_3 from Shubnikov-de Haas effect, *Phys. Status Solidi B* **74**, 591 (1976).
- [13] H. Köhler, Anisotropic g -factor of the conduction electrons in Bi_2Te_3 , *Phys. Status Solidi B* **75**, 127 (1976).
- [14] V. A. Kulbachinskii, M. Inoue, M. Sasaki, H. Negishi, W. X. Gao, K. Takase, Y. Gimán, P. Lostak, and J. Horak, Valence-band energy spectrum of solid solutions of narrow-gap-semiconductor $\text{Bi}_{2-x}\text{Sn}_x\text{Te}_3$ single crystals, *Phys. Rev. B* **50**, 16921 (1994).
- [15] C. W. Rischau, B. Leridon, B. Fauqué, V. Metayer, and C. J. van der Beek, Doping of Bi_2Te_3 using electron irradiation, *Phys. Rev. B* **88**, 205207 (2013).
- [16] Z. Alpichshev, J. G. Analytis, J.-H. Chu, I. R. Fisher, Y. L. Chen, Z. X. Shen, A. Fang, and A. Kapitulnik, STM Imaging of Electronic Waves on the Surface of Bi_2Te_3 : Topologically Protected Surface States and Hexagonal Warping Effects, *Phys. Rev. Lett.* **104**, 016401 (2010).
- [17] C. Chen, S. He, H. Weng, W. Zhang, L. Zhao, H. Liu, X. Jia, D. Mou, S. Liu, J. He, Y. Peng, Y. Feng, Z. Xie, G. Liu, X. Dong, J. Zhang, X. Wang, Q. Peng, Z. Wang, S. Zhang, F. Yang, C. Chen, Z. Xu, X. Dai, Z. Fang, and X. J. Zhou, Robustness of topological order and formation of quantum well states in topological insulators exposed to ambient environment, *Proc. Natl. Acad. Sci.* **109**, 3694 (2012).
- [18] J. Sánchez-Barriga, M. R. Scholz, E. Golias, E. Rienks, D. Marchenko, A. Varykhalov, L. V. Yashina, and O. Rader, Anisotropic effect of warping on the lifetime broadening of topological surface states in angle-resolved photoemission from Bi_2Te_3 , *Phys. Rev. B* **90**, 195413 (2014).
- [19] P.-Y. Chuang, S.-H. Su, C.-W. Chong, Y.-F. Chen, Y.-H. Chou, J.-C.-A. Huang, W.-C. Chen, C.-M. Cheng, K.-D. Tsuei, C.-H. Wang, Y.-W. Yang, Y.-F. Liao, S.-C. Weng, J.-F. Lee, Y.-K. Lan, S.-L. Chang, C.-H. Lee, C.-K. Yang, H.-L. Su, and Y.-C. Wu, Anti-site defect effect on the electronic structure of a Bi_2Te_3 topological insulator, *RSC Adv.* **8**, 423 (2018).
- [20] Y.-Y. Li, G. Wang, X.-G. Zhu, M.-H. Liu, C. Ye, X. Chen, Y.-Y. Wang, K. He, L.-L. Wang, X.-C. Ma, H.-J. Zhang, X. Dai, Z. Fang, X.-C. Xie, Y. Liu, X.-L. Qi, J.-F. Jia, S.-C. Zhang, and Q.-K. Xue, Intrinsic topological insulator Bi_2Te_3 thin films on Si and their thickness limit, *Adv. Mater.* **22**, 4002 (2010).
- [21] I. G. Austin, The optical properties of bismuth telluride, *Proc. Phys. Soc.* **72**, 545 (1958).
- [22] R. Sehr and L. Testardi, The optical properties of p -type Bi_2Te_3 - Sb_2Te_3 alloys between 2–15 microns, *J. Phys. Chem. Solids* **23**, 1219 (1962).
- [23] D. Greenaway and G. Harbeke, Band structure of bismuth telluride, bismuth selenide and their respective alloys, *J. Phys. Chem. Solids* **26**, 1585 (1965).
- [24] G. A. Thomas, D. H. Rapkine, R. B. Van Dover, L. F. Mattheiss, W. A. Sunder, L. F. Schneemeyer, and J. V. Waszczak, Large electronic-density increase on cooling a layered metal: Doped Bi_2Te_3 , *Phys. Rev. B* **46**, 1553 (1992).
- [25] R. Vilaplana, O. Gomis, F. J. Manjón, A. Segura, E. Pérez-González, P. Rodríguez-Hernández, A. Muñoz, J. González, V. Marín-Borrás, V. Muñoz-Sanjosé, C. Drasar, and V. Kucek, High-pressure vibrational and optical study of Bi_2Te_3 , *Phys. Rev. B* **84**, 104112 (2011).
- [26] B. C. Chapler, K. W. Post, A. R. Richardella, J. S. Lee, J. Tao, N. Samarth, and D. N. Basov, Infrared electrodynamics and ferromagnetism in the topological semiconductors Bi_2Te_3 and Mn-doped Bi_2Te_3 , *Phys. Rev. B* **89**, 235308 (2014).
- [27] A. Dubroka, O. Caha, M. Hronček, P. Friš, M. Orlita, V. Holý, H. Steiner, G. Bauer, G. Springholz, and J. Humlíček, Interband absorption edge in the topological insulators $\text{Bi}_2(\text{Te}_{1-x}\text{Se}_x)_3$, *Phys. Rev. B* **96**, 235202 (2017).
- [28] F. C. Peiris, E. T. Holmgren, J. W. Lyons, X. Li, X. Liu, M. Dobrowolska, and J. K. Furdyna, Optical properties of $\text{Bi}_2(\text{Te}_{1-x}\text{Se}_x)_3$ thin films, *J. Vac. Sci. Technol. B* **37**, 031205 (2019).
- [29] S. K. Mishra, S. Satpathy, and O. Jepsen, Electronic structure and thermoelectric properties of bismuth telluride and bismuth selenide, *J. Phys.: Condens. Matter* **9**, 461 (1997).
- [30] S. J. Youn and A. J. Freeman, First-principles electronic structure and its relation to thermoelectric properties of Bi_2Te_3 , *Phys. Rev. B* **63**, 085112 (2001).
- [31] P. Larson, Effect of $p_{1/2}$ corrections in the electronic structure of Bi_2Te_3 compounds, *Phys. Rev. B* **68**, 155121 (2003).
- [32] G. Wang and T. Cagin, Electronic structure of the thermoelectric materials Bi_2Te_3 and Sb_2Te_3 from first-principles calculations, *Phys. Rev. B* **76**, 075201 (2007).
- [33] O. V. Yazyev, E. Kioupakis, J. E. Moore, and S. G. Louie, Quasiparticle effects in the bulk and surface-state bands of Bi_2Se_3 and Bi_2Te_3 topological insulators, *Phys. Rev. B* **85**, 161101(R) (2012).
- [34] I. Aguilera, C. Friedrich, G. Bihlmayer, and S. Blügel, *GW* study of topological insulators Bi_2Se_3 , Bi_2Te_3 and Sb_2Te_3 : Beyond the perturbative one-shot approach, *Phys. Rev. B* **88**, 045206 (2013).
- [35] I. A. Nechaev and E. V. Chulkov, Quasiparticle band gap in the topological insulator Bi_2Te_3 , *Phys. Rev. B* **88**, 165135 (2013).
- [36] M. Michiardi, I. Aguilera, M. Bianchi, V. E. de Carvalho, L. O. Ladeira, N. G. Teixeira, E. A. Soares, C. Friedrich, S. Blügel, and P. Hofmann, Bulk band structure of Bi_2Te_3 , *Phys. Rev. B* **90**, 075105 (2014).
- [37] I. Aguilera, C. Friedrich, and S. Blügel, Many-body corrected tight-binding Hamiltonians for an accurate quasiparticle description of topological insulators of the Bi_2Se_3 family, *Phys. Rev. B* **100**, 155147 (2019).
- [38] O. Caha, A. Dubroka, J. Humlíček, V. Holý, H. Steiner, M. Ul-Hassan, J. Sánchez-Barriga, O. Rader, T. N. Stanislavchuk, A. A. Sirenko, G. Bauer, and G. Springholz, Growth, structure,

- and electronic properties of epitaxial bismuth telluride topological insulator films on BaF₂ (111) substrates, *Cryst. Growth Des.* **13**, 3365 (2013).
- [39] H. Steiner, V. Volobuev, O. Caha, G. Bauer, G. Springholz, and V. Holý, Structure and composition of bismuth telluride topological insulators grown by molecular beam epitaxy, *J. Appl. Crystallogr.* **47**, 1889 (2014).
- [40] P. Kacman and W. Zawadzki, Spin magnetic moment and spin resonance of conduction electrons in α -Sn-type semiconductors, *Phys. Status Solidi B* **47**, 629 (1971).
- [41] W. Zawadzki, Semirelativity in semiconductors, *High Magn. Fields Phys. Semiconduct.* **2**, 755 (1997).
- [42] M. O. Goerbig, G. Montambaux, and F. Piéchon, Measure of Diracness in two-dimensional semiconductors, *Europhys. Lett.* **105**, 57005 (2014).
- [43] M. Orlita, B. A. Piot, G. Martinez, N. K. S. Kumar, C. Faugeras, M. Potemski, C. Michel, E. M. Hankiewicz, T. Brauner, Č. Drašar, S. Schreyeck, S. Grauer, K. Brunner, C. Gould, C. Brüne, and L. W. Molenkamp, Magneto-Optics of Massive Dirac Fermions in Bulk Bi₂Se₃, *Phys. Rev. Lett.* **114**, 186401 (2015).
- [44] W. Zawadzki, Semirelativity in semiconductors: A review, *J. Phys.: Condens. Matter* **29**, 373004 (2017).
- [45] O. Ly and D. M. Basko, Theory of electron spin resonance in bulk topological insulators Bi₂Se₃, Bi₂Te₃ and Sb₂Te₃, *J. Phys.: Condens. Matter* **28**, 155801 (2016).
- [46] C.-X. Liu, X.-L. Qi, H. J. Zhang, X. Dai, Z. Fang, and S.-C. Zhang, Model Hamiltonian for topological insulators, *Phys. Rev. B* **82**, 045122 (2010).
- [47] M. Orlita, P. Neugebauer, C. Faugeras, A.-L. Barra, M. Potemski, F. M. D. Pellegrino, and D. M. Basko, Cyclotron Motion in the Vicinity of a Lifshitz Transition in Graphite, *Phys. Rev. Lett.* **108**, 017602 (2012).
- [48] A. Wolos, S. Szyszko, A. Drabinska, M. Kaminska, S. G. Strzelecka, A. Hruban, A. Materna, and M. Piersa, Landau-Level Spectroscopy of Relativistic Fermions with Low Fermi Velocity in the Bi₂Te₃ Three-Dimensional Topological Insulator, *Phys. Rev. Lett.* **109**, 247604 (2012).
- [49] V. A. Kulbachinskii, N. Miura, H. Arimoto, T. Ikaida, P. Lostak, H. Horak, and C. Drasar, Cyclotron resonance in high magnetic fields in Bi₂Se₃, Bi₂Te₃ and Sb₂Te₃ based crystals, *J. Phys. Soc. Jpn.* **68**, 3328 (1999).
- [50] F. M. Peeters and J. T. Devreese, Energy levels of two- and three-dimensional polarons in a magnetic field, *Phys. Rev. B* **31**, 3689 (1985).
- [51] F. M. Peeters and J. T. Devreese, Magneto-optical absorption of polarons, *Phys. Rev. B* **34**, 7246 (1986).
- [52] A. M. Witowski, M. Orlita, R. Stępniewski, A. Wysmołek, J. M. Baranowski, W. Strupiński, C. Faugeras, G. Martinez, and M. Potemski, Quasiclassical cyclotron resonance of Dirac fermions in highly doped graphene, *Phys. Rev. B* **82**, 165305 (2010).
- [53] W. Richter and C. R. Becker, A raman and far-infrared investigation of phonons in the rhombohedral V₂-VI₃ compounds Bi₂Se₃, Bi₂Te₃ and Sb₂Te₃ and Bi₂(Te_{1-x}Se_x)₃ (0 < x < 1), (Bi_{1-y}Sb_y)₂Te₃ (0 < y < 1), *Phys. Status Solidi B* **84**, 619 (1977).
- [54] V. B. Berestetskii, E. M. Lifshitz, and L. P. Pitaevskii, *A Course of Theoretical Physics* (Pergamon, New York, 1977), Vol. 3, p. 455.
- [55] Y. Izaki and Y. Fuseya, Nonperturbative Matrix Mechanics Approach to Spin-Split Landau Levels and the g Factor in Spin-Orbit Coupled Solids, *Phys. Rev. Lett.* **123**, 156403 (2019).
- [56] M. H. Cohen and E. I. Blount, The g-factor and de Haas-van Alphen effect of electrons in bismuth, *Philos. Mag.* **5**, 115 (1960).
- [57] A. Wolos, A. Drabinska, S. Szyszko, M. Kaminska, S. G. Strzelecka, A. Hruban, A. Materna, and M. Piersa, Three-dimensional topological insulators Bi₂Te₃, Bi₂Se₃, and Bi₂Te₂Se—A microwave spectroscopy study, *AIP Conf. Proc.* **1566**, 197 (2013).
- [58] P. Drath and G. Landwehr, Band parameters and g-factor for n-type Bi₂Te₃ from the Schubnikov-De Haas effect, *Phys. Lett. A* **24**, 504 (1967).
- [59] L. M. Roth, B. Lax, and S. Zwerdling, Theory of optical magneto-absorption effects in semiconductors, *Phys. Rev.* **114**, 90 (1959).
- [60] J. R. Drabble, Galvanomagnetic effects in p-type bismuth telluride, *Proc. Phys. Soc.* **72**, 380 (1958).
- [61] E. Burstein, Anomalous optical absorption limit in InSb, *Phys. Rev.* **93**, 632 (1954).
- [62] G. Martinez, B. Piot, M. Hakl, M. Potemski, Y. Hor, A. Materna, S. Strzelecka, A. Hruban, O. Caha, J. Novák *et al.*, Determination of the energy band gap of Bi₂Se₃, *Sci. Rep.* **7**, 6891 (2017).
- [63] P. Y. Yu and M. Cardona, *Fundamentals of Semiconductors: Physics and Materials Properties* (Springer, Berlin, 1996).
- [64] B. A. Bernevig, T. L. Hughes, and S.-C. Zhang, Quantum spin Hall effect and topological phase transition in HgTe quantum wells, *Science* **314**, 1757 (2006).
- [65] M. König, S. Wiedmann, C. Brüne, A. Roth, H. Buhmann, L. W. Molenkamp, X.-L. Qi, and S.-C. Zhang, Quantum spin Hall insulator state in HgTe quantum wells, *Science* **318**, 766 (2007).
- [66] M. Orlita, K. Masztalerz, C. Faugeras, M. Potemski, E. G. Novik, C. Brüne, H. Buhmann, and L. W. Molenkamp, Fine structure of zero-mode Landau levels in HgTe/Hg_xCd_{1-x}Te quantum wells, *Phys. Rev. B* **83**, 115307 (2011).
- [67] B. A. Assaf, T. Phuphachong, E. Kampert, V. V. Volobuev, P. S. Mandal, J. Sánchez-Barriga, O. Rader, G. Bauer, G. Springholz, L. A. de Vaulchier, and Y. Guldner, Negative Longitudinal Magnetoresistance from the Anomalous $N = 0$ Landau Level in Topological Materials, *Phys. Rev. Lett.* **119**, 106602 (2017).
- [68] G. Krizman, B. A. Assaf, M. Orlita, T. Phuphachong, G. Bauer, G. Springholz, G. Bastard, R. Ferreira, L. A. de Vaulchier, and Y. Guldner, Avoided level crossing at the magnetic field induced topological phase transition due to spin-orbital mixing, *Phys. Rev. B* **98**, 161202(R) (2018).
- [69] M. Cardona, *Solid State Physics* (Academic, New York, 1969), Chap. Modulation Spectroscopy, Suppl. 11.
- [70] P. Lautenschlager, M. Garriga, S. Logothetidis, and M. Cardona, Interband critical points of GaAs and their temperature dependence, *Phys. Rev. B* **35**, 9174 (1987).
- [71] J. Humlíček and M. Garriga, *Silicon-Germanium Carbon Alloys Growth, Properties and Applications* (Taylor & Francis, New York, 2002), Chap. Temperature Dependence of the Optical Spectra of Si_{1-x}Ge_x Alloys, p. 483.
- [72] J. E. Rowe and D. E. Aspnes, Approximate Treatment of Exciton Effects in Electric Field Modulation Via the Slater-Koster Interaction, *Phys. Rev. Lett.* **25**, 979 (1970).